Prediction of Flowfields About Bodies of Revolution at Large Incidence

K.-Y. Chien,* A. H. Van Tuyl,† and T. Hsieh*
Naval Surface Weapons Center, Silver Spring, Maryland

A comparative study of flows past a slightly blunted ogive-cylinder at 10 deg incidence and a hemisphere-cylinder at 19 deg incidence has been conducted using a thin-layer Navier-Stokes model and a three-dimensional inviscid vortex filament model. Separation lines obtained from the former model were used as input to calculations made using the latter. Also included in the comparison is a classical boundary-layer calculation due to Cebeci using the potential-flow solution as the given external inviscid flow.

Nomenclature

C_p = pressure coefficient
D = body diameter
M_∞ = freestream Mach number
p = pressure
R = $D/2$
Re = Reynolds number, $= U_\infty D/\nu$
U_∞ = freestream velocity
t = time
x,y,z = Cartesian coordinate system
α = angle of attack
ϵ_E, ϵ_I = explicit and implicit dissipation coefficients, respectively; $\epsilon_I = 3\epsilon_E$
θ = azimuthal angle as measured from the windward plane of symmetry
ν = kinematic viscosity
ξ,η,ζ = coordinates in the computational domain
ρ = fluid density

I. Introduction

PREDICTION of aerodynamic characteristics of missiles at large incidence has become increasingly important because of the requirement of high maneuverability. The flowfield about this type of body at large incidence is very complicated due to the strong viscous-inviscid interaction and three-dimensional flow separation. Many inviscid models for predicting such flows, including the use of vortex filaments,[1] point vortices,[2] or Euler equations,[3] assume that viscous effects in the separated region can be approximately taken into account by imposing a separation line which is given by experiment or other theoretical calculation.[4-6] However, experimental data are usually expensive and time-consuming to obtain, and, thus, are frequently not available when needed. Among the theoretical methods for determining the separation line, the most popular is the classical boundary-layer theory which, in the incompressible case, uses the potential-flow solution to describe the surface pressure distribution and external inviscid flow. For problems with rather extensive flow separation, the validity of the potential-flow solution becomes questionable, and some compliciated iterative procedure may be required to take into account the viscous-inviscid interaction process properly.

Recently, it has become possible to simulate the three-dimensional separated flowfield by solving the compressible time-dependent Navier-Stokes equations in the thin-layer approximation.[7,8] Such an approach includes viscous effects, and should lead to a better prediction of the flowfield. However, large amounts of computer time and storage are required; thus, inviscid models are still widely used because of their simplicity. Therefore, a comparative study to determine the relative merits and limitations of the viscous and inviscid models is desirable. Herein, thin-layer Navier-Stokes solutions have been obtained using the code developed by Pulliam and Steger[7] at a nearly incompressible condition ($M_\infty = 0.2$) for two cases: 1) a 10% spherically blunted three-caliber ogive-cylinder at 10 deg incidence, and 2) a hemisphere-cylinder at 19 deg incidence. Laminar flow was assumed. The flowfield was also computed using an extension of the incompressible inviscid vortex filament model of Ref. 1, based on the separation lines obtained from the thin-layer Navier-Stokes solutions. In addition, Cebeci has kindly provided us with the incompressible boundary-layer results for the first case based on the method of Ref. 6. The purpose of this paper is to present detailed comparisons of the results as predicted by these methods.

In Sec. II, the thin-layer Navier-Stokes model and the inviscid vortex filament model are described. In Sec. III, similarities and differences between results obtained using these numerical models are discussed. Finally, some conclusions and remarks concerning these comparisons are given in Sec. IV.

II. Numerical Models

Thin-Layer Navier-Stokes Model

The numerical method used for solving the thin-layer approximation of the three-dimensional, unsteady, compressible Navier-Stokes equations is described in Refs. 7 and 9. The governing equations are written in a strong conservation-law form. A general coordinate transformation is used to map the physical domain into a rectangular computational domain (see Fig. 1). The finite difference numerical method used is the implicit approximate factorization algorithm of Beam and Warming.[9] Using second-order accurate time differencing, the finite difference equations are split into three sets of one-dimensional equations in each of the computational directions ξ, η, and ζ. These equations are applied to the interior points in the computational domain and give a block (5×5) tridiagonal system of equations that can be solved by the LU decomposition method. Fourth-order accurate differencing is used for the convection terms to prevent the truncation error from exceeding the magnitude of the viscous terms themselves. Second-order implicit and fourth-order explicit artificial dissipation terms are added to improve the numerical stability of the method.

As shown in Fig. 1, the boundary conditions are implemented as follows: 1) on the body surface, $u = v = w = 0$; 2)

Presented as Paper 84-0506 at the AIAA 22nd Aerospace Sciences Meeting, Reno, NV, Jan. 9-12, 1984; received Jan. 31, 1984; revision received Oct. 3, 1985.

*Aerospace Engineer. Associate Fellow AIAA.
†Mathematician. Member AIAA.

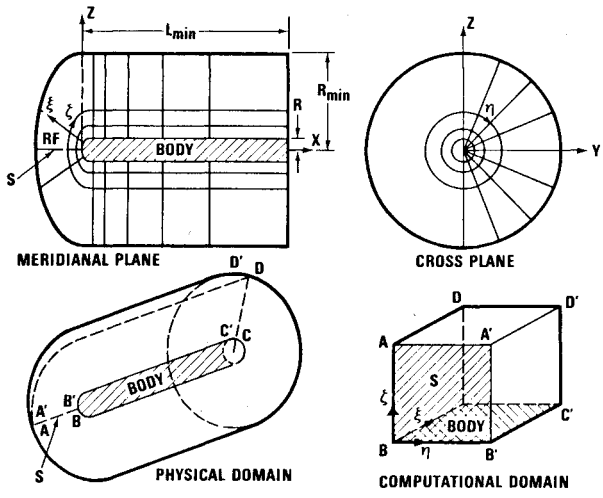

Fig. 1 Coordinate system.

at the far-field boundaries, the constant freestream values are specified; 3) on the downstream boundary, the pressure is fixed at p_∞, and ρ, u, v, and w are extrapolated; 4) on the singular line (AB or S in Fig. 1), flow variables are extrapolated and an average is taken; 5) on the plane of symmetry (pitch plane), the reflection principle is used. The flow variables on the boundaries are updated explicitly.

The numerical code used herein is the vectorized version of the AIR3D Code developed by Pulliam and Steger.[7] The computations were carried out on the CRAY-1 computer of the Air Force Weapons Laboratory (AFWL). It is found that the vectorized code using the CRAY-1 computer is approximately 11 times faster than the nonvectorized code using the CDC 7600 computer.

Calculations have been carried out using the thin-layer Navier-Stokes (TLNS) model for a 10% spherically blunted, three-caliber ogive-cylinder at 10 deg incidence and for a hemisphere-cylinder at 19 deg incidence, for laminar flow at $M_\infty = 0.2$ and $Re = 10^5$. The grid distribution used is 36 (meridional direction) $\times$ 21 (circumferential direction) $\times$ 32 (normal direction), covering a region defined by $RF/D = 3.61$, $L_{min}/D = 11$, and $R_{min}/D = 6.5$ (see Fig. 1) in the first problem, and by the corresponding values 1.5, 5, and 6 in the second problem. The starting time step was set equal to 0.001, and was gradually increased to a final value of 0.1. This final time step was maintained until the steady state was reached. The ratio $\epsilon_E/\Delta t$ was set equal to 10 at early times and gradually decreased to 1. The ratio ϵ_I/ϵ_E was always set equal to 3. A uniform flow was used as the initial condition, and a steady-state condition was reached after about 1000 time steps. Each time step took about 3 s on the AFWL CRAY-1 computer.

Inviscid Vortex Filament Model

Steady incompressible potential flow is assumed, with a given smooth separation line of open type on each side of the body. In the present method, the condition of tangential flow on the body is satisfied by use of quadrilateral source panels. A constant source density is determined on each quadrilateral so that the normal component of velocity vanishes at the null point. The latter is the point at which the velocity induced by the quadrilateral is normal to the plane of the quadrilateral. Nearly identical results were obtained when the centroid was used instead of the null point. The positions of the quadrilaterals are adjusted as shown in Fig. 2, where portions of sections consisting of two rings each are rotated, so that the given separation line passes through the null points of selected quadrilaterals. Quadrilaterals were not placed on the base of the cylinder, and no attempt was made to model the base flow. The vortex wake is approximated by a given number of segmented three-dimensional vortex filaments, each ending in a semi-infinite filament parallel to the freestream, and

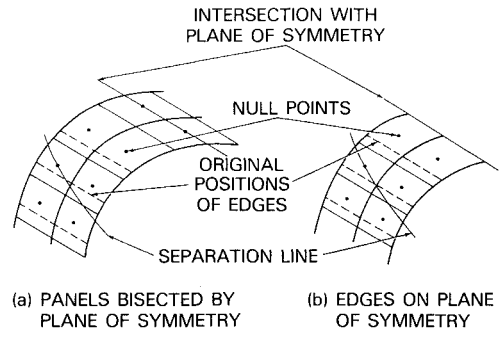

Fig. 2 Adjustment of quadrilaterals.

attached to the body at a null point. Each pair of symmetrically placed vortex filaments is connected by a segment inside the body to produce a horseshoe-type vortex.

The present method is an iterative one in which the calculation of circulations and source densities is alternated with a roll-up calculation. In the former calculation, the vortex filament shapes are held fixed, and the circulations and source densities are calculated simultaneously by an iterative procedure. In the latter, circulations and source densities are held fixed while the orientations of the filaments are computed by an iterative roll-up calculation. The filaments are initially taken to be straight and parallel to the freestream.

In the calculation of the circulations, use is made of the conditions at the juncture of a separating vortex sheet and the body. Assuming that vorticity is shed from the body into the vortex sheet, it is shown in Ref. 10 that the following conditions hold:

1) The vortex sheet is tangent to the body.

2) The separation line is a streamline on the downstream side of the vortex sheet, while the velocity at the separation line on the upstream side of the separation line is equal to the upstream velocity on the body.

These conditions, together with the continuity of velocity magnitude (speed) across the vortex sheet, are sufficient for the calculation of the variation of circulation along the separation line in terms of the upstream velocity on the body. This calculation is used as part of a finite difference procedure for determining the circulations of the filaments. More details are given in Ref. 11.

Calculations have been carried out by the vortex filament method for each of the preceding cases, using analytical least-squares fits to the separation lines obtained from the TLNS calculations. The quadrilateral configurations corresponding to Figs. 2a and 2b will be referred to in the following as QD1 and QD2, respectively. The spherical portion of each body was covered by 24 quadrilaterals on each side of the plane of symmetry in both QD1 and QD2. The separation line for both problems begins after the spherical portion of the body and, hence, it is not necessary to rotate quadrilaterals there. The total number of quadrilaterals on the blunted ogive-cylinder in the configuration QD1 was 408 without symmetry and 234 when symmetry was taken into account. The corresponding numbers of quadrilaterals on the hemisphere-cylinder were 312 and 176. In configuration QD2, the number of quadrilaterals on one side of the plane of symmetry was 204 in the case of the blunted ogive-cylinder and 156 in the case of the hemisphere-cylinder. The number of filaments on one side of the body was 12 in the former case and 9 in the latter for both QD1 and QD2. Each filament consisted of 17 segments of unequal lengths.

In each case, the calculation was carried out for a total of 14 roll-up iterations. The sources and circulations were first calculated with the filaments parallel to the freestream. The roll-up calculation was then carried out for seven iterations, and the sources and circulations were recalculated using the most recent filament shapes. The roll-up calculation was then carried out for seven more iterations, and a final calculation of source strengths and circulations was made.

III. Results and Discussion

Figure 3 compares the surface pressure distribution on the blunted ogive-cylinder in the meridional direction obtained from the TLNS solution with that corresponding to the potential-flow solution used in the boundary-layer calculations. The two pressure distributions are seen to be qualitatively similar. However, the fact that the pressures on the windward ($\theta = 0$ deg) and leeward ($\theta = 180$ deg) meridians become equal in the downstream direction in the case of the potential-flow solution indicates that the use of the latter is questionable when separation is present.

The surface flow pattern of the limiting streamlines obtained using the TLNS model is shown in Fig. 4 by plotting the direction and relative magnitude of the skin friction at each grid point on the body surface. Note that on the leeside ($\theta = 180$ deg), the meridional component of the skin friction (which is equal to the total skin friction there) is always pointed in the downstream direction. This signifies an open type of separation as classified by Wang.[5] A separation line which is the envelope of the limiting streamlines coming from both sides is shown as a broken line in Fig. 4. It is entirely on the cylindrical afterbody and is rather flat.

Shown in Fig. 5 is a comparison between this separation line and that given by the boundary-layer solution. Unlike the TLNS solution, a closed-type separation which starts from the leeside on the ogive part of the body is predicted by the boundary-layer solution of Cebeci et al.[6]

Further comparisons between the two theories are made by examining the angle that a limiting streamline makes with the local meridional line. This angle is termed the surface flow angle, γ_w. Figure 6 gives the distribution of γ_w in the circumferential direction at several fixed x locations as calculated by both theories. Boundary-layer theory gives no solution in the separated region, where the TLNS model does not seem to have any particular difficulty. Furthermore, a somewhat sharper downward turn is predicted by the boundary-layer solution as the separation line is reached when compared to the TLNS solution. Except for these differences, both results are seen to be qualitatively quite similar.

Comparisons between the TLNS solution and the inviscid vortex filament method have also been made. The circumferential surface pressure distributions at several longitudinal stations on the blunted ogive-cylinder are shown in Fig. 7. Also shown is the potential-flow solution obtained by the same method but with the vortex filaments omitted (no vortices). At $x/D = 0.9$ and 2, which lie upstream of the beginning of flow separation, it can be seen that the results of the inviscid vortex filament model are nearly identical with the potential-flow solutions. Also, close agreement between the inviscid vortex filament and TLNS models is found except near $\theta = 0$ and 180 deg. At $x/D = 3.8$ and 7.5, the largest discrepancy between the results obtained by the vortex filament and TLNS models is found near $\theta = 0$ deg. The vortex filament results are nearly identical with those obtained by the potential-flow calculations except near $\theta = 180$ deg, where the former are in good agreement with the TLNS results, and the potential-flow solutions are higher.

Figure 8 shows the meridional pressure distributions on a blunted ogive-cylinder calculated at $\theta = 0$, 90, and 180 deg. The vortex filament calculations were carried out using only the configuration QD1. The pressures at $\theta = 90$ deg were obtained by quadratic interpolation, since the quadrilaterals with centroids originally at $\theta = 90$ deg were rotated during calculation of quadrilateral input data as in Fig. 2a. When $\theta = 0$ deg,

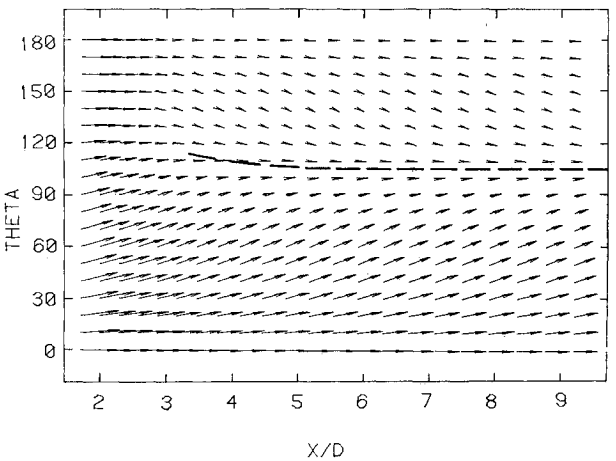

Fig. 4 Surface flow pattern on a 10% blunted ogive-cylinder at 10 deg incidence as determined from the skin friction vector distribution.

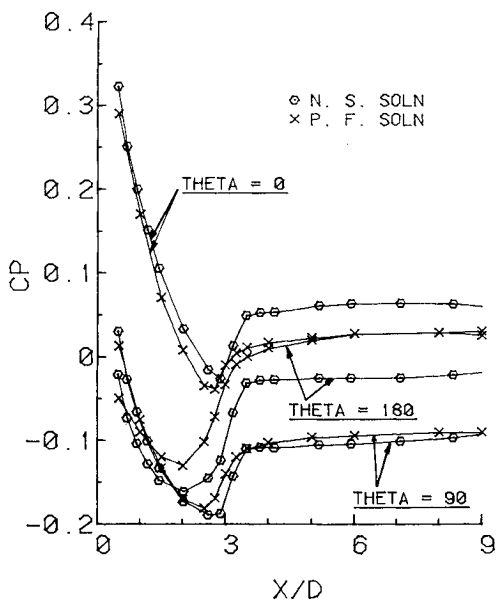

Fig. 3 Meridional pressure distributions on a 10% blunted ogive-cylinder at 10 deg incidence.

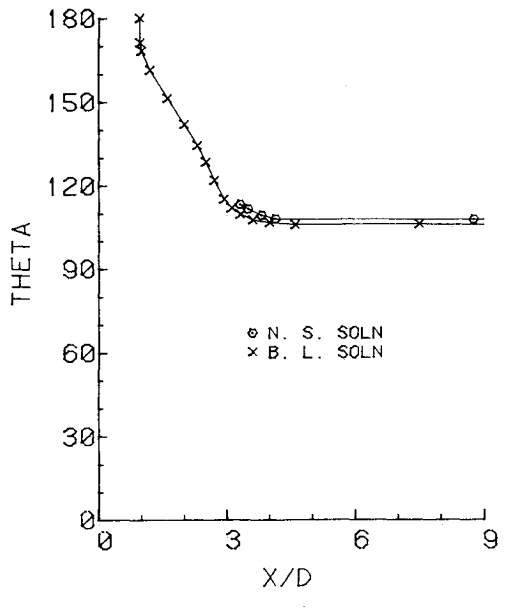

Fig. 5 Comparison of lines of separation on a 10% blunted ogive-cylinder at 10 deg incidence between the thin-layer Navier-Stokes solution and the boundary-layer solution.

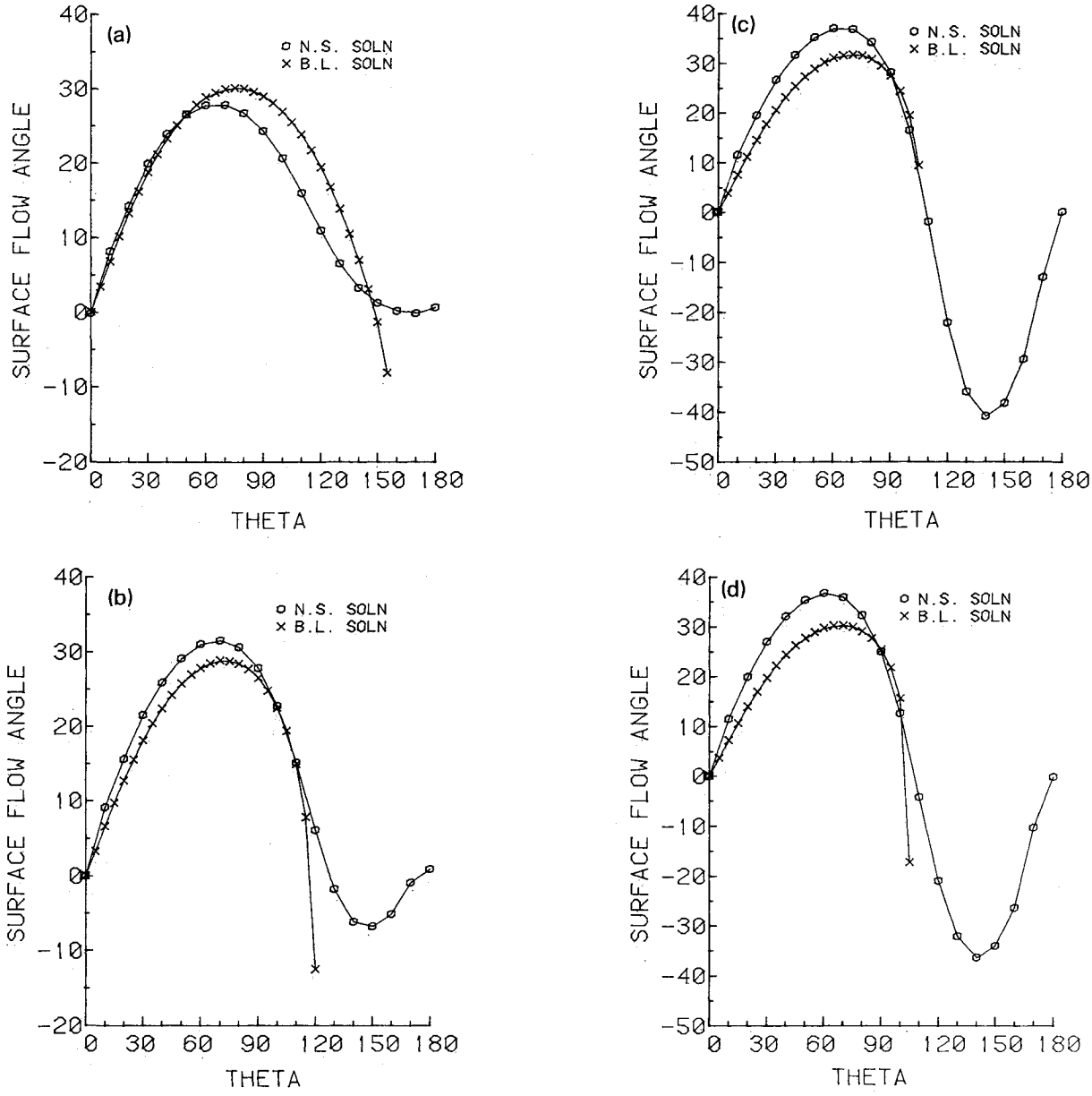

Fig. 6 Comparison of surface flow angle distributions on a 10% blunted ogive-cylinder at 10 deg incidence; a) $x/D=1.2$, b) $x/D=2.6$, c) $x/D=3.8$, d) $x/D=9.2$.

it can be seen that the pressures calculated by the vortex filament method nearly coincide with the potential-flow values, and that they are lower than the values obtained by the TLNS model over most of the body by a nearly constant amount. At $\theta=90$ deg, the pressures obtained by the TLNS model nearly coincide with the potential-flow pressures throughout, while the pressures calculated by the vortex filament method are slightly higher on the back part of the body. At $\theta=180$ deg, good agreement is found between the pressures calculated by the vortex filament model and the results of the TLNS model on the back part of the body, while the potential-flow pressures are much higher.

The separation line on the cylindrical afterbody of the hemisphere-cylinder calculated by the TLNS model is shown in Fig. 9. It should be mentioned that there is also a nose separation bubble near the shoulder region of the hemisphere-cylinder. Since the nose separation bubble is not amenable to the inviscid vortex filament method, only the open-type separation line shown in Fig. 9 is used in this calculation. In Fig. 10, meridional pressure distributions on a hemisphere-cylinder at 19 deg incidence, obtained by the TLNS and vortex filament models and the potential-flow calculations, are shown. The trends observed in Fig. 10 are found to be similar to those of the blunted ogive-cylinder results of Fig. 8.

Also shown in Fig. 10 are experimental data at $M_\infty=0.6$, which is the lowest Mach number at which results were obtained in Ref. 12. Assuming that compressibility effects at this Mach number are insignificant, one may conclude that the data agree best with the inviscid results on the windward side ($\theta=0$ deg), and with the TLNS solution at $\theta=90$ and 180 deg. The reason for the overprediction of the surface pressure by the TLNS model at $\theta=0$ deg is not currently understood. In Ref. 8, for the same geometry but with $M_\infty=1$, the TLNS solution, inviscid results, and experimental data were found to be in better agreement at $\theta=0$ deg than in the present case. Unfortunately, lack of funding has prevented the authors from investigating this discrepancy any further. However, good agreement with experimental data at both $\theta=90$ and 180 deg suggests that the TLNS solutions reported herein are not unreasonable.

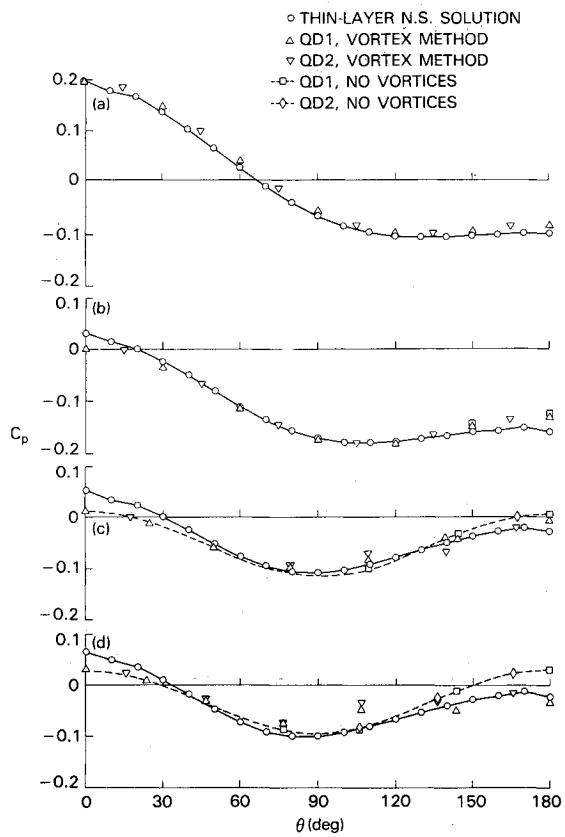

Fig. 7 Circumferential pressure distributions on a 10% blunted ogive-cylinder at 10 deg incidence; a) $x/D=0.9$, b) $x/D=2.0$, c) $x/D=3.8$, d) $x/D=7.5$.

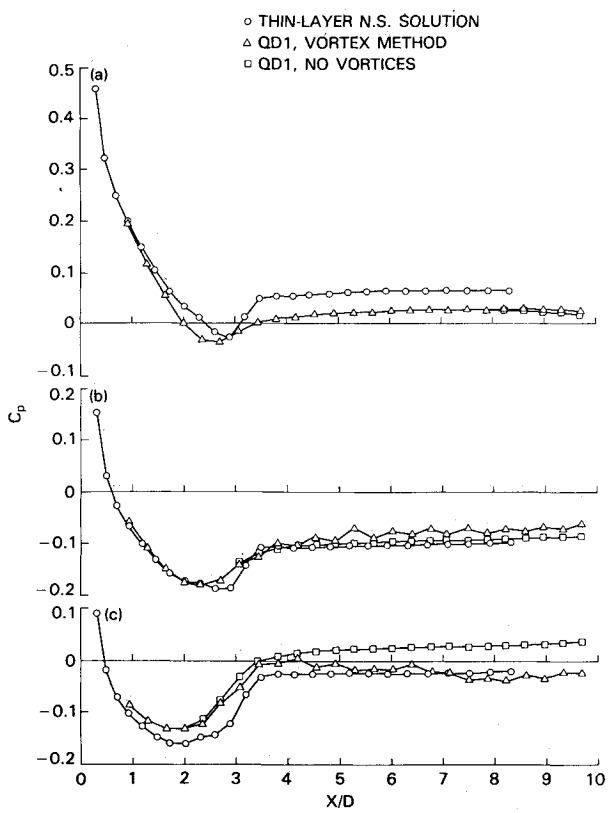

Fig. 8 Meridional pressure distributions on a 10% blunted ogive-cylinder at 10 deg incidence; a) $\theta=0$ deg, b) $\theta=90$ deg, c) $\theta=180$ deg.

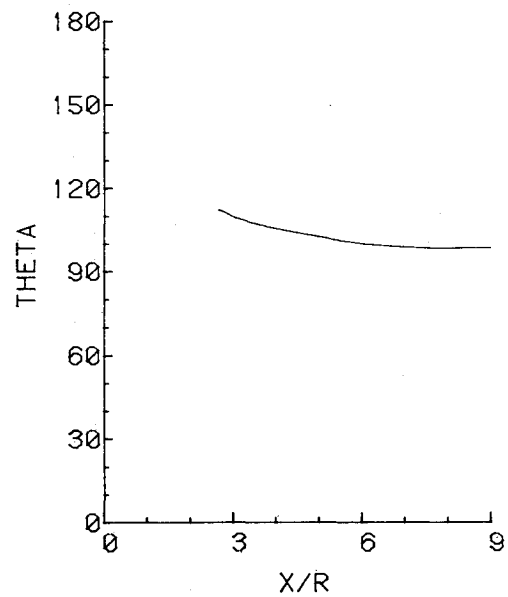

Fig. 9 Separation line on the cylindrical afterbody of a hemisphere-cylinder at 19 deg incidence.

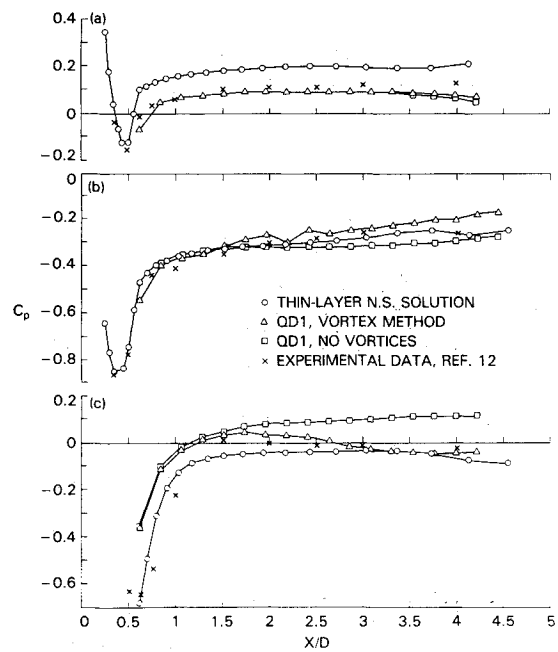

Fig. 10 Meridional pressure distributions on a hemisphere-cylinder at 19 deg incidence; a) $\theta=0$ deg, b) $\theta=90$ deg, c) $\theta=180$ deg.

IV. Concluding Remarks

Numerical calculations of laminar flows over a slightly blunted ogive-cylinder at 10 deg incidence and a hemisphere-cylinder at 19 deg incidence have been carried out using the thin-layer Navier-Stokes code of Pulliam and Steger.[7] The surface flow pattern obtained in the former case has been compared with that given by the boundary-layer solution of Cebeci et al.[6] The striking difference is that the Navier-Stokes solution yields an open-type separation, whereas the boundary-layer solution predicts a closed-type separation. The compressible thin-layer Navier-Stokes code of Pulliam and Steger seems to produce reasonable results even in the nearly incompressible flow regime, but the amounts of computer time and storage required for such calculations are very large.

Results have also been obtained using a three-dimensional inviscid vortex filament model. Surface pressure distributions so obtained have been compared with the thin-layer Navier-Stokes solutions and the potential-flow calculations. For both cases studied, the inclusion of the vortex filaments in the potential-flow model improves the agreement with the results of the thin-layer Navier-Stokes calculations on the leeward side ($\theta = 180$ deg) on the back part of the body, but leads to results essentially identical to those of classical potential theory on the windward side ($\theta = 0$ deg).

Acknowledgments

This work was sponsored by the Naval Sea Systems Command under the cognizance of L. Pasiuk, the Naval Air Systems Command under the cognizance of D. E. Hutchins, and the Naval Surface Weapons Center Independent Research Program. Thanks are extended to T. Cebeci and K. Kaups, Douglas Aircraft Company, for providing their boundary-layer results, and to J. Benek, Calspan Field Service Inc. (AEDC), for providing the vectorized version of the AIR3D Code.

References

[1]Van Tuyl, A. H., "Three-Dimensional Calculation of Vortices Behind a Missile at Large Angles of Attack," *Boundary-Layer Effects—Proceedings of the 7th U.S. Air Force/FRG Data Exchange Agreement Meeting,* AFFDL-TR-78-111, 1978, pp. 340-349.

[2]Wardlaw, A. B. Jr., "Multivortex Model of Asymmetric Shedding on Slender Bodies at High Angle of Attack," AIAA Paper 75-123, Jan. 1975.

[3]Klopfer, G. H. and Nielsen, J. N., "Euler Solutions of the Body Vortices of Tangent Ogive Cylinders at High Angles of Attack and Supersonic Speeds," AIAA Paper 81-0361, Jan. 1981.

[4]Marshall, F. J. and Deffenbaugh, F. D., "Separated Flow Over a Body of Revolution," *Journal of Aircraft*, Vol. 12, Feb. 1975, pp. 78-85.

[5]Wang, K. C., "Separation Patterns of Boundary-Layer Over an Inclined Body of Revolution," *AIAA Journal*, Vol. 10, Aug. 1971, pp. 1044-1050.

[6]Cebeci, T., Khattab, A. A., and Stewartson, K., "Three-Dimensional Laminar Boundary Layers and the Ok of Accessibility," *Journal of Fluid Mechanics,* Vol. 107, 1981, pp. 57-87.

[7]Pulliam, T. H. and Steger, J. L., "Implicit Finite Difference Simulations of Three-Dimensional Compressible Flow," *AIAA Journal*, Vol. 18, Feb. 1980, pp. 159-167.

[8]Hsieh, T., "Calculation of Viscous, Sonic Flow Over Hemisphere-Cylinder at 19 Degrees Incidence: The Capturing of Nose Vortices," AIAA Paper 81-0189, Jan. 1981.

[9]Beam, R. M. and Warming, R. F., "An Implicit Factored Scheme for the Compressible Navier-Stokes Equations," *AIAA Journal*, Vol. 16, April 1978, pp. 393-402.

[10]Smith, J. H. B., "Behavior of a Vortex Sheet Separating from a Smooth Surface," RAE TR 77058, April 1977.

[11]Van Tuyl, A. H., "A Vortex Filament Model of the Wake behind a Missile at High Angle of Attack," to be submitted to the *AIAA Journal.*

[12]Hsieh, T., "An Investigation of Separated Flow about a Hemisphere-Cylinder at 0 to 19 Degree Incidence in the Mach Number Range from 0.6 to 1.5," AEDC-TR-76-112, Nov. 1976.